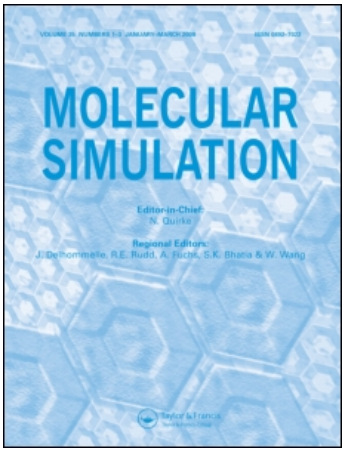

Molecular Simulation
Publication details, including instructions for authors and subscription information:
http://www.informaworld.com/smpp/title~content=t713644482

Simulation studies of methane, carbon dioxide, hydrogen and deuterium in ITQ-1 and NaX zeolites

George K. Papadopoulos[a]; Doros N. Theodorou[a]
[a] School of Chemical Engineering, National Technical University of Athens, Athens, Greece

First published on: 21 September 2010

To cite this Article Papadopoulos, George K. and Theodorou, Doros N.(2009) 'Simulation studies of methane, carbon dioxide, hydrogen and deuterium in ITQ-1 and NaX zeolites', Molecular Simulation, 35: 1, 79 — 89, First published on: 21 September 2010 (iFirst)
To link to this Article: DOI: 10.1080/08927020802468380
URL: http://dx.doi.org/10.1080/08927020802468380

Molecular Simulation
Vol. 35, Nos. 1–2, January–February 2009, 79–89

Taylor & Francis
Taylor & Francis Group

Simulation studies of methane, carbon dioxide, hydrogen and deuterium in ITQ-1 and NaX zeolites

George K. Papadopoulos[1] and Doros N. Theodorou*

School of Chemical Engineering, National Technical University of Athens, 157 80 Athens, Greece

(*Received 23 July 2008; final version received 8 September 2008*)

The sorption dynamics of methane, carbon dioxide, hydrogen and deuterium in digitally reconstructed frameworks of ITQ-1 and NaX zeolites were investigated via atomistic and mesoscopic computer simulations. The loading dependence of self-diffusivity proved to be affected by the energetic inhomogeneity of the sorption sites or/and their topology in the particular crystal. Collective (Maxwell–Stefan) and hence transport diffusivities are examined on the basis of sorbate–sorbate interactions via a jump diffusion model invoking quasi-chemical mean field theory.

Keywords: molecular dynamics; NaX; ITQ-1; hydrogen; carbon dioxide

1. Introduction

The efficient design of nanoporous sorbents for reaction, separation or environmental engineering processes requires a systematic study of the dynamical properties of sorbate molecules confined in the interior of these materials, which may be either crystalline or amorphous. This type of study typically deals with a multicomponent sorbed phase inside a porous crystalline (e.g. zeolites) or amorphous (e.g. carbon molecular sieves, carbon nanotubes) sorbent material; under the conditions used in the majority of the applications, the solid phase can be considered static without seriously affecting the microscopic flow dynamics of the system [1].

Apart from the strong technology-oriented incentives for studying the dynamics of fluids in pore systems, revealing the physical aspects affecting the transport of the sorbed phase is of great fundamental interest. Among many classes of solids, which serve as sorbent materials, structures exhibiting a high degree of order in their atomic-level structure, such as zeolites, and more recently zeolitic shape-persistent analogues, such as zeolite imidazolate, metal- or covalent-organic frameworks and titanosilicates, have proved particularly promising. The significant advantage of these materials lies in their well-defined structural characteristics, namely the channel size and shape, the micropore connectivity and the charge distribution due, for example, to the presence of more than one kind of tetrahedral (T) atoms in their framework.

Following the macroscopic phenomenological approach, mass transport is studied in terms of flux vectors generated by density or chemical potential gradients in the sorbed phase by invoking either Fick's laws or Maxwell–Stefan theory and the Onsager formulation, respectively [1–3]. The microscopic modelling of diffusion, on the other hand, involves mostly deterministic molecular dynamics (MD) simulations in equilibrium or non-equilibrium MD ensembles. Atomistic MD cannot address time scales longer than microseconds with currently available computational means. In order to overcome this problem, in the cases where transport occurs as a sequence of infrequent jumps between sites in the nanoporous medium, an alternative way is to identify the sites where penetrant molecules spend most of their time, compute intersite transition rates atomistically based on infrequent event theory and sample stochastic trajectories consisting of long sequences of jumps by kinetic Monte Carlo (KMC) simulation. KMC can clearly cover longer time scales; its use presupposes a time-scale separation between the time required for a molecule to equilibrate within a state, and the waiting time before a jump to another state occurs. Theodorou et al. [1] and references therein describe in detail the methodology and the applicability of dynamically corrected transition state theory in conjunction with KMC to diffusion studies of molecules sorbed in zeolites.

In this article, we describe an attempt to relate the sorption and diffusion properties of fluids such as hydrogen, methane, carbon dioxide and their mixtures in pure siliceous and in anionic aluminosilicate zeolite frameworks containing interstitial and exchangeable cations. We apply MD and proceed by utilising the relationship of transport coefficients and time correlation functions under the equilibrium *NVE* ensemble, employing the Onsager regression hypothesis as it was later reformulated in the context of linear response theory [4]. The treatment of transport phenomena via atomistic simulation has the

*Corresponding author. Email: doros@central.ntua.gr

ISSN 0892-7022 print/ISSN 1029-0435 online

DOI: 10.1080/08927020802468380
http://www.informaworld.com

advantage, in comparison with macroscopic phenomenology, of predicting diffusivity magnitudes, as well as their temperature, loading and composition dependencies. Also, the predicted results are amenable to comparison with mesoscopic and microscopic experimental measurements, such as pulsed field gradient NMR and quasi-elastic neutron scattering, respectively, which have been carried out on a variety of zeolite–guest systems [5–9].

2. Computer modelling

2.1 Zeolite digitisation

The procedure we followed for reconstructing a digital crystal entails adopting the unit cell geometric characteristics that correspond to the particular framework-type code; locating the position vectors of the 'primary' framework atoms [10], from the X-ray diffraction pattern or neutron diffraction data of the crystal; and then applying the symmetry operations of the space group to which the crystal belongs. The types and position vectors of all framework and off-framework atoms of the unit cell, taking into account their occupancy probability found from the XRD analysis or neutron diffraction data, are finally generated to form a computer model of the unit cell.

We constructed a model for the ITQ-1 zeolite framework by employing a double unit cell instead of the original hexagonal one, for convenience with periodic boundary conditions. This new unit cell has an orthorhombic shape with axes $a = 2\sin(60°)a'$ $b = a'$; $c = c'$, where a' and c' are the original hexagonal unit cell axes. This procedure gave rise to a base-centred orthorhombic unit cell comprising 144 silicon and 288 oxygen atoms, with lattice points located at the centres of large cavities of the zeolite [11].

The Si/Al ratio in the framework of the charged NaX ($Na_{86}Al_{86}Si_{106}O_{384}$) FAU crystal not only determines the anionic charge per unit cell and thereby the number of cations, but also affects the distribution of cations among the various kinds of sites present in the unit cell. Because the Al and Si atoms are indistinguishable by the XRD technique, in several positions the occupation probability for either type of T atom is less than unity. The notation for the topology of these sites and their occupancy by sodium cations have been reported in [10]. In this study, we used the model of Jaramillo and Auerbach [12], which explicitly distinguishes the Si and Al atoms, attributing different partial charges to the oxygen framework atoms according to their neighbouring bonded T atoms. With this objective, we randomly distributed Al atoms among the T sites of the framework up to the desired Si/Al ratio, in such a way that Löwenstein's rule was fulfilled. In addition, the energy of the crystal was minimised by means of a simulated annealing technique (Figure 1).

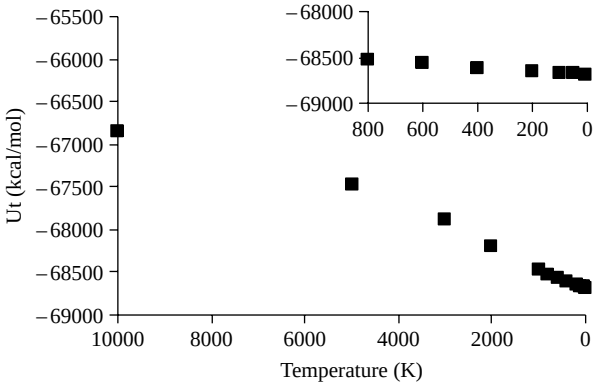

Figure 1. Indicative total energy plateau during the simulated annealing minimisation procedure in NaY [10]; the last runs locating the minimum global energy of the crystal are depicted in the inset.

The representation of the bed of NaX crystals discussed in Section 3 was obtained using a mesoscopic particle-based reconstruction method, where a prescribed porosity and particle size are provided experimentally. The NaX final configuration was arrived at through a successive series of energy minimisations by means of molecular mechanics at constant particle number density. In this work, the zeolite bed consists of octahedral NaX crystals, based on the experimentally measured bed density of $590\,\mathrm{kg\,m^{-3}}$, the crystal density of $1530\,\mathrm{kg\,m^{-3}}$ and the porosity of 0.6; the mean crystal size (edge length of the platonic octahedra) was equal to $30\,\mu\mathrm{m}$ [8].

2.2 Guest–host interactions

The triatomic linear molecule of carbon dioxide was modelled as two consecutive dumb-bells sharing the central C atom, arranged on a straight line; partial charges were distributed around each molecule so as to reproduce experimental quadrupole moments [13]. The octapole moment of the methane molecule was ignored; thus, methane was represented as one neutral Lennard-Jones sphere with the following parameters: $\varepsilon_{CH_4-CH_4}/k_B = 102.5\,\mathrm{K}$, $\sigma_{CH_4-CH_4} = 0.362\,\mathrm{nm}$; $\varepsilon_{CH_4-O}/k_B = 131.2\,\mathrm{K}$, $\sigma_{CH_4-O} = 0.346\,\mathrm{nm}$; and $\varepsilon_{CH_4-Na}/k_B = 328.3\,\mathrm{K}$, $\sigma_{CH_4-Na} = 0.294\,\mathrm{nm}$. The above values resulted from performing a calibration with respect to measured sorption isotherms; they are able to reproduce satisfactorily a set of experimental data in a temperature range from 120 to 550 K found in [14]. Hydrogen was also modelled as a single Lennard-Jones site; its strength and size parameters resulted from calibration with respect to bulk experimental data, as explained in [7,9] and the references therein.

For the short-ranged sorbate–sorbate and sorbate–zeolite atom interactions, the Lennard-Jones potential was used, whereas for hydrogen, the approximation due

to Feynman and Hibbs [15] was employed for all dispersion-type interactions involved, in order to account for its quantum nature, i.e.

$$U_q(r_{ij}) = U_{\mathrm{LJ}}(r_{ij}) + \frac{\hbar^2}{24 m_r k_B T}\left[\frac{\partial^2 U_{\mathrm{LJ}}(r_{ij})}{\partial r_{ij}^2} + \frac{2}{r_{ij}}\frac{\partial U_{\mathrm{LJ}}(r_{ij})}{\partial r_{ij}}\right], \quad (1)$$

where $U_{\mathrm{LJ}}(r)$ is the Lennard-Jones potential function and m_r is the reduced mass of the interacting pair of atoms, given by $m_r^{-1} = M_j^{-1} + M_i^{-1}$; M denotes molecular mass and subscripts specify the pair interaction type, e.g. H_2—H_2 ($i = j$) or H_2 with any atom in the zeolite framework ($i \neq j$).

The long-ranged electrostatic interactions were handled by means of the Ewald summation technique; the parameters used for the real and reciprocal parts of the sums, as well as the values of partial charges on the sorbate molecules and framework atoms have been reported in detail elsewhere [10]. In order to reduce the computational effort associated with both the short- and long-ranged sorbate–sorbent interactions, when the sorbent was modelled as a rigid framework of atoms, as in the case of the zeolite crystals studied in this work, we pretabulated these interactions prior to the actual simulation run on a fine grid running through the pore space of the sorbent. Sorbate–sorbate interactions, on the other hand, were computed explicitly at each step.

Sorption equilibria were studied by means of grand canonical Monte Carlo (GCMC) simulations. These simulations also provided the starting configurations for our MD simulations of transport. In the case of the faujasite NaX, we need to avoid stochastic formation of the CO_2 and H_2 molecules inside sodalite cages during GCMC. Sodalite cages are voluminous enough to accommodate one of these sorbate molecules; yet, they are inaccessible to these molecules in reality, since the apertures connecting them to the main pore space are too small to be traversed by the sorbates at any reasonable rate. After the pretabulation of the entire potential, the interior of sodalite cages was excluded from the sampling procedure during the Monte Carlo runs; thus, the sampling of intra-crystalline space was confined to the physically acceptable regions that are determined by the sizes of the CO_2 and H_2 molecules, on the one hand, and openings of the sodalite framework, on the other hand. Figure 2 shows our computation of the electrostatic field within a certain plane in the NaX unit cell.

The density, ρ, of sorbate molecules in the zeolite unit cells was computed by means of GCMC sampling in the form of phase space averages under an imposed set of chemical potential, μ, volume, V, and temperature, T, values. In particular, the version of the GCMC algorithm due to Adams adopted here involves the quantity B, which

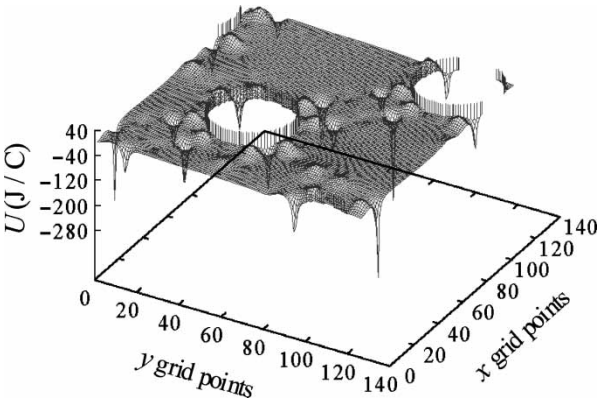

Figure 2. Indicative computed electrostatic field contours for NaX, at $z = 2.27$ nm. The sodalite interiors, which are removed from the mapping, are evident as open circular regions.

is related to the excess chemical potential μ^{ex} of the sorbed phase through the relation

$$B = \frac{1}{k_B T}\mu^{\mathrm{ex}} + \ln\langle N\rangle, \quad (2)$$

while B is related to fugacity, f, of the bulk phase being in equilibrium with the sorbed phase according to the equation

$$Vf = k_B T \exp(B), \quad (3)$$

with k_B being the Boltzmann constant. In the remainder of this work, fugacity is approximated by the pressure, assuming that the bulk phase behaves nearly as an ideal gas.

2.3 *Transport*

The simulations of both methane and xenon were carried out in the standard MD *NVE* ensemble. The MD method creates a set of classical trajectories by integrating the equations of motion for a group of molecules within a fixed volume of zeolite. The equations of motion were formulated in the Cartesian coordinates for all sorbate atoms. The sorbate molecules followed classical trajectories, whose time evolution was governed by Newton's equation of motion; the neglect of quantum effects is fully justified at the temperatures of interest here except for H_2, whose interactions are described by correcting the potentials as described above. The algorithms chosen for the solution of the differential equations of motion for all sorbates studied in this work belong to the category of Störmer–leapfrog integrators.

For the linear molecule of CO_2, the LEN algorithm [13,16] was applied. It is a leapfrog algorithm in the sense that the quantities saved between time steps are the on-step orientation and the mid-step angular velocity. In particular, in place of angular velocity the rate of change of the bond

vector, **u**, is used. Synoptically, if $\hat{\mathbf{e}}$ is the unit bond vector fixed along the molecule axis, the torque **T** on the molecule can be written as

$$\mathbf{T} = \sum_{\alpha} \mathbf{r}_{\alpha} \times \mathbf{f}_{\alpha} = \hat{\mathbf{e}} \times \sum_{\alpha} d_{\alpha} \mathbf{f}_{\alpha} = \hat{\mathbf{e}} \times \mathbf{g}, \tag{4}$$

with **g** being the 'turning force', which can be determined from the non-bonded forces $\mathbf{f}_{\alpha}$ on each atom, the position vectors $\mathbf{r}_{\alpha}$ of each interaction site and the (algebraic) distances d_{α} of each atom α from the centre of mass of the linear molecule. In a linear molecule, **g** can be replaced by its component perpendicular to the molecular axis, $\mathbf{g}_{\mathrm{p}}$, without affecting the torque. The component $\mathbf{g}_{\mathrm{p}}$ is defined as

$$\mathbf{g}_{\mathrm{p}} = \mathbf{g} - (\hat{\mathbf{e}} \cdot \mathbf{g})\hat{\mathbf{e}}. \tag{5}$$

In order to avoid the use of angular velocity, the time derivative of the axis vector was used

$$\mathbf{u} = \frac{\mathrm{d}\hat{\mathbf{e}}}{\mathrm{d}t} \tag{6}$$

In this algorithm, we applied the constraint that the length of the $\hat{\mathbf{e}}$ vector remains unity by means of an undetermined Lagrange multiplier [16]. LEN showed remarkable stability, being capable of admitting very large time steps.

The elaboration of MD results towards the estimation of transport coefficients, as mentioned in Section 1, relies on linear response theory, which provides the bridge between equilibrium time correlation functions and non-equilibrium response to weak perturbations. The theory also proves that the time integrals of autocorrelation functions are related to transport coefficients via the relations known as Green–Kubo. In an averaged form that allows accumulating statistics over all the N molecules of the system possessing centre-of-mass velocities, $\mathbf{v}_a$, where $a = 1, \ldots, N$, and for a three-dimensional system, these relations take the following forms for the self-diffusivity, D_{s}, and the collective diffusivity, D_0, respectively:

$$D_{\mathrm{s}} = \frac{1}{3N} \int_0^{\infty} \mathrm{d}t \left\langle \sum_{i=1}^{N} \mathbf{v}_i(t) \cdot \mathbf{v}_i(0) \right\rangle, \tag{7}$$

$$D_0 = \frac{1}{3N} \int_0^{\infty} \mathrm{d}t \sum_{i=1}^{N} \sum_{j=1}^{N} \langle \mathbf{v}_i(t) \cdot \mathbf{v}_j(0) \rangle. \tag{8}$$

Alternatively, the above equations are usually used in their equivalent well-known Einstein form involving the position vectors of the particles, $\mathbf{r}_i$, i.e.

$$D_{\mathrm{s}} = \frac{1}{6N} \lim_{t \to \infty} \frac{\mathrm{d}}{\mathrm{d}t} \left\langle \sum_{i=1}^{N} [\mathbf{r}_i(0) - \mathbf{r}_i(t)]^2 \right\rangle, \tag{9}$$

$$D_0 = \frac{1}{6N} \lim_{t \to \infty} \frac{\mathrm{d}}{\mathrm{d}t} \left\langle \left[\sum_{i=1}^{N} [\mathbf{r}_i(0) - \mathbf{r}_i(t)] \right]^2 \right\rangle. \tag{10}$$

A general expression for the isothermal steady-state single-component sorbate flow in the absence of external force fields can be written in the Fickian form as follows:

$$\mathbf{J} = -\mathbf{D}_{\mathrm{t}}(\rho) \cdot \nabla \rho. \tag{11}$$

In the above equation, the vector **J** is the overall macroscopic flux, expressed as the mean number of molecules flowing per unit cross-sectional area in a directional (anisotropic) medium due to a concentration (number density ρ) gradient, and $\mathbf{D}_{\mathrm{t}}$ is the transport diffusivity tensor, which in general can be a function of concentration. Therefore, in zeolite crystals or textured materials, transport and, consequently, self- and collective diffusivity have a tensorial character (the reader is reminded that Equations (7)–(10) are orientational averages); in other words, the flux vector depends on the spatial orientation of the applied density gradient with respect to the crystal symmetry axes. In an isotropic medium, Equation (11) converts to the well-known Fick's law defining the scalar diffusivity.

The relationship between the (orientationally averaged) transport and collective diffusivity can be expressed through a Darken-type equation, i.e.

$$D_t(\rho) = D_0(\rho) \frac{\partial \ln f}{\partial \ln \rho}. \tag{12}$$

In the preceding lines, we have followed the Fickian phenomenological approach to linking fluxes and concentration gradients. The interested reader can find an analogous phenomenological development based on chemical potential gradients due to Onsager, as well as the Stefan–Maxwell formulation, which is based on a balance of forces exerted on the diffusing particles, in Refs [17,18] and references therein.

3. Results and discussion

In this section, we present results on sorption and diffusion computer experiments on selected siliceous and charged zeolite frameworks. Comparisons with experimental measurements are made, whenever possible.

The sorbed phase concentration (loading) inside the crystal was computed by means of grand canonical ensemble Monte Carlo. Figure 3 shows the sorption isotherms of methane and carbon dioxide in ITQ-1 for

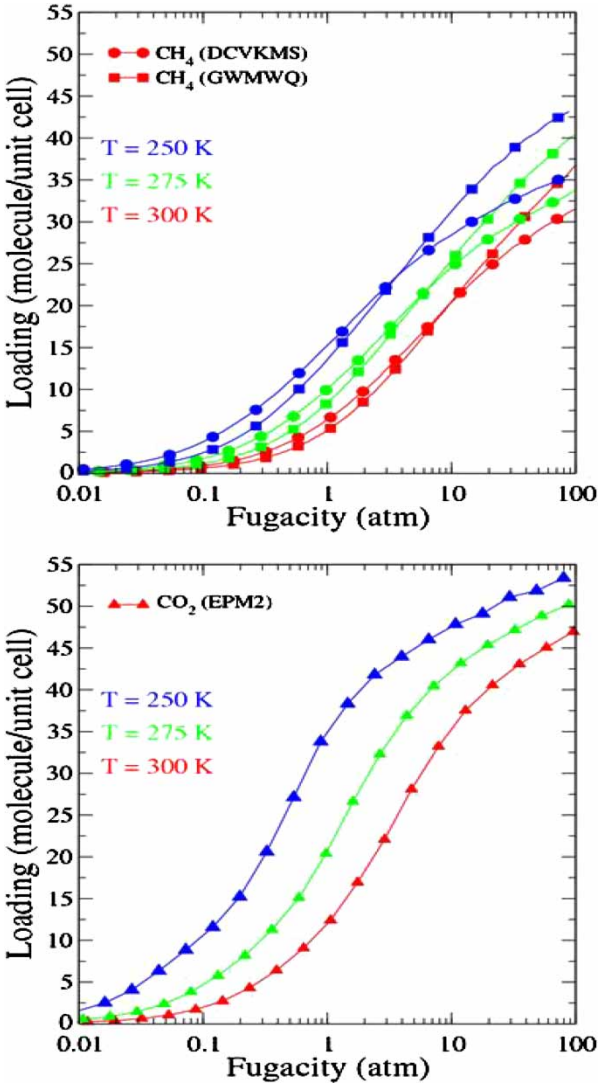

Figure 3. Sorption isotherms of CH_4 for two sets of parameters [19,20] and of the EPM2 model of CO_2 [21] at various temperatures within ITQ-1.

various sets of parameters used to describe the energetics of these systems in previous studies.

The singlet density distribution $\rho^1(\mathbf{r}_1)$ for finding a molecule of methane at a certain position $\mathbf{r}_1$, averaged over all occupancies and all configurations, $\mathbf{r} = \{\mathbf{r}_1, \mathbf{r}_2, \ldots, \mathbf{r}_N\}$, inside the unit cell, given by the relation,

$$\rho^1(\mathbf{r}_1) = \frac{1}{\Xi(\mu, V, T)} \sum_{N=1}^{\infty} \frac{\exp[\mu N / k_B T]}{(N-1)!} \int d^3 r_2 \cdots d^3 r_N \times \exp[-U(\mathbf{r})/k_B T], \tag{13}$$

is depicted in Figure 4; in this figure, we selected low-value isodensity surfaces in order to depict the accessible (void) volume, indicating the two independent pore systems (large cavity, LC; sinusoidal channel, SC) of this zeolite.

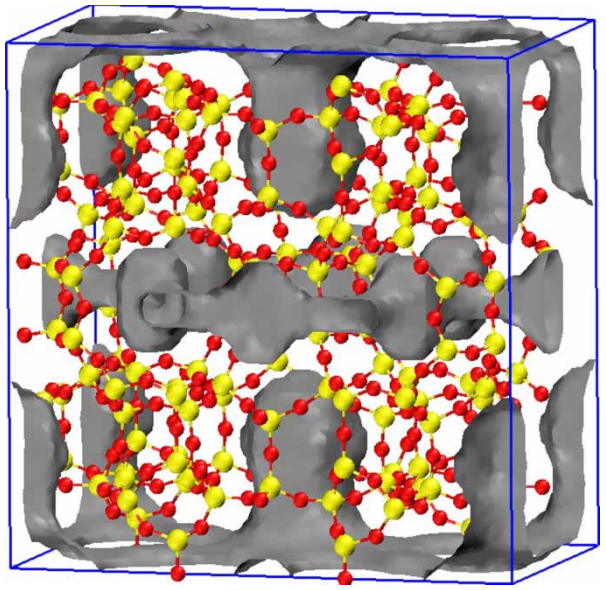

Figure 4. Lowest value isodensity surface of CH_4 in ITQ-1 at a total loading of 20.4 (LC) plus 8.6 (SC) molecules per unit cell.

In Figure 5, the experimentally measured sorption isotherms showing the results of GCMC simulation for methane in faujasite X zeolite ($Na_{86}X$) are presented for two temperatures; the location of sorbed methane molecules in the interior of supercages in a snapshot from the simulation is depicted in Figure 6.

Figure 7 presents the sorption isotherms of hydrogen and deuterium in $Na_{86}X$ at 100 K. All the host–guest and guest–guest dispersive interactions have been described by means of the Feynman–Hibbs potential mentioned in the previous section; the effect of the quantum correction tends to reduce the well depth and shift the whole potential function to the right, increasing the effective size of the sorbed molecules. In particular, the lighter hydrogen molecule has a bigger effective size with weaker energy interaction than deuterium. This relative difference

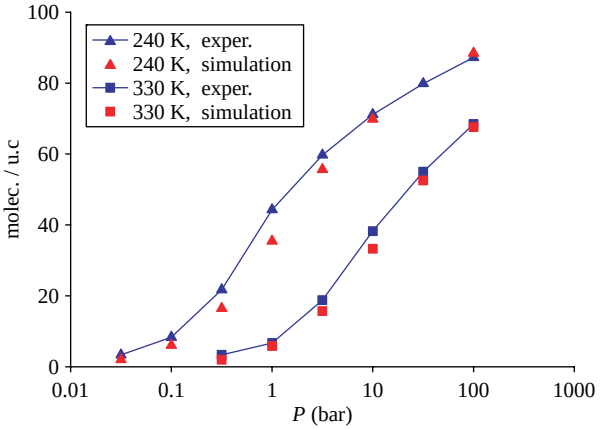

Figure 5. Measured [14] and predicted sorption isotherms of CH_4 in NaX.

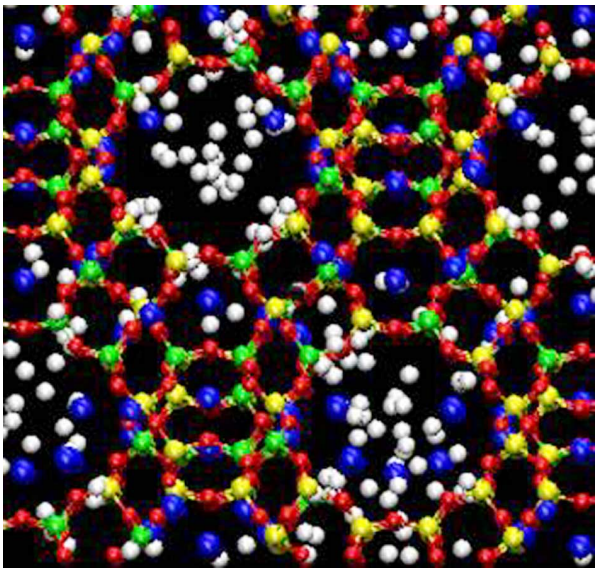

Figure 6. Distribution of CH_4 (white spheres) in the $Na_{86}X$ framework, depicting the host sorption areas (supercages) at a loading of 9.16 molecules per supercage at 300 K.

is depicted in Figure 7, where deuterium is seen to be sorbed slightly more strongly than hydrogen.

In Figure 8, self-diffusivity measurements of methane obtained from pulsed field gradient NMR at 223 K [22] and 300 K [23] in faujasite X zeolite ($Na_{86}X$) are shown, along with the results of MD under the same conditions.

Predicted and measured values agree reasonably well, indicating a decrease in the intra-crystalline CH_4 self-diffusivity as the concentration of sorbed phase increases inside the NaX. The PFG-NMR and MD values appear significantly different at the higher temperature, whereas the agreement at 223 K is more satisfactory. PFG-NMR can also sample the inter-crystalline space in addition to the crystal interior, which is solely sampled by MD. Kärger et al. [22] and Caro et al. [23] state that the molecular exchange between the crystallites and the

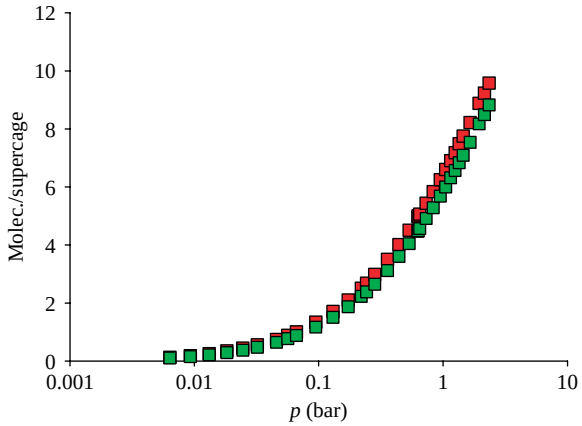

Figure 7. Simulated sorption isotherms at 100 K for D_2 (red symbols) and H_2 (green symbols) in NaX.

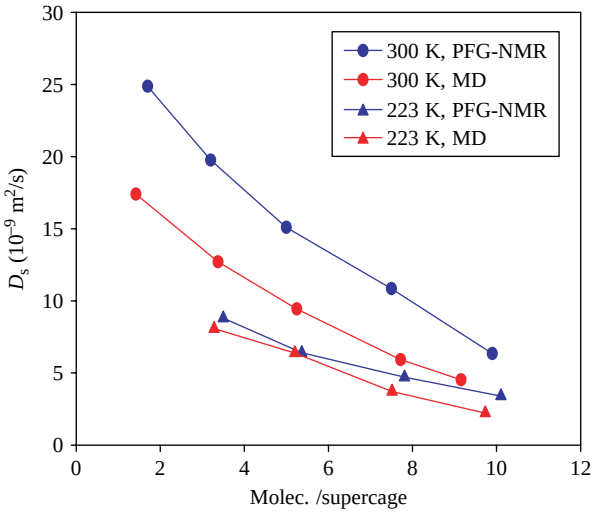

Figure 8. Comparison of self-diffusivity data obtained via PFG-NMR measurements at 223 [22] and 300 K [23], with molecular dynamics simulations for CH_4 in NaX as a function of loading.

inter-crystalline space during the observation time was negligible; hence, the measured signal can be solely attributed to the intra-crystalline motion. Therefore, the discrepancy at the higher temperature may not be attributed to the different length scales probed by PFG-NMR and MD. In previous studies [8,24], it was shown that no matter what the intra-crystalline diffusivity is, a major contribution to the measured effective diffusivity must be expected from the inter-crystalline diffusivity, as well as from the fraction of molecules in the inter-crystalline space around the crystallites; both quantities are highly temperature dependent.

In Figure 9, results from KMC simulation of inter-crystalline diffusivity of ethane in a bed of NaX crystals as a function of the (pressure and temperature dependent) mean free path in the gas phase are shown. The whole procedure of our KMC involves collisions of molecules in the inter-crystalline space only, being treated in a mean field sense without explicitly considering colliding pairs. The distance l travelled between successive collisions is picked from an exponential distribution under the prevailing temperature T and pressure p; that is random trajectories are generated in the void space of the medium in such a way that in the bulk gas the lengths l between successive collisions follow the exponential distribution expected from the Poisson stochastic sequence of intermolecular collisions [8], i.e., $\langle l \rangle f(l) = \exp(-l/\langle l \rangle)$, where $f(l)\mathrm{d}l$ is the conditional probability of having a collision-free trajectory length between l and $l + \mathrm{d}l$, with the mean value of l being denoted by $\langle l \rangle$. In the bulk gas phase, $\langle l \rangle$ is the molecular mean free path $\lambda = k_B T / p\sigma_{gas}^2 \pi\sqrt{2}$, with σ_{gas} being the collision diameter of gas molecules. Reflections upon collision with the isotropic crystal surface are assumed to be diffuse, i.e. a new direction of motion is generated according to the

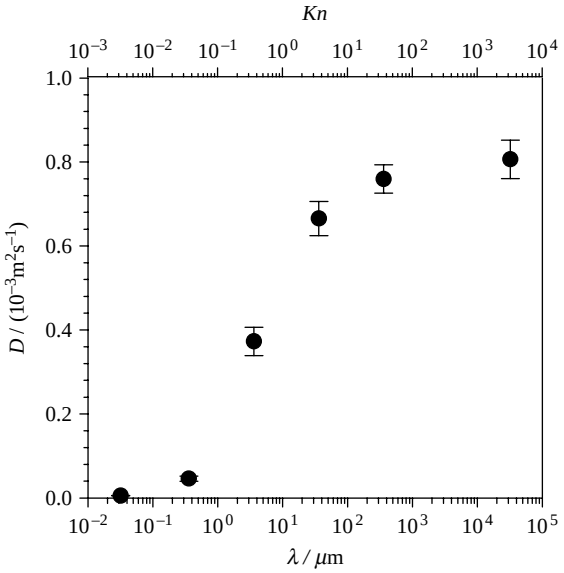

Figure 9. Inter-crystalline self-diffusivity of C_2H_6 computed via kinetic Monte Carlo simulation in a reconstructed bed of octahedral NaX crystals with porosity 0.40 as a function of mean free path λ.

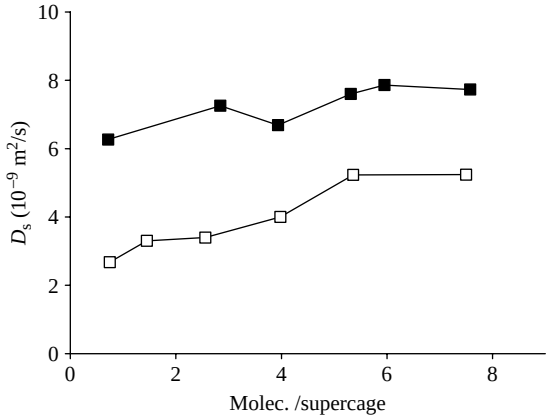

Figure 10. Self-diffusivities of D_2 in NaX measured by QENS at 100 K [9] (open symbols), and results computed by MD under the same conditions (filled symbols) as a function of sorbate loading.

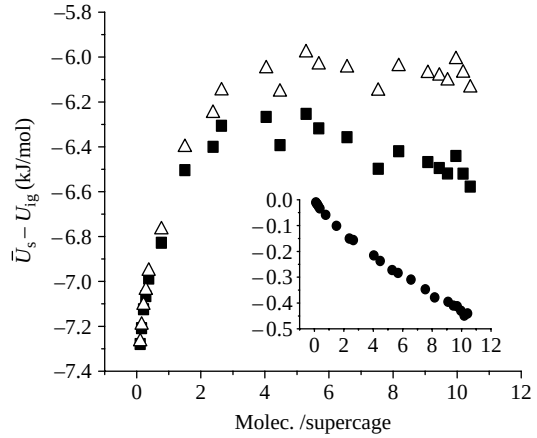

Figure 11. Partial molar configurational internal energy of sorbed H_2 in NaX calculated from GCMC simulations at a temperature of 100 K and various loadings (squares), and contributions to this quantity from H_2–NaX interactions (triangles) and from H_2–H_2 interactions (inset) are also shown.

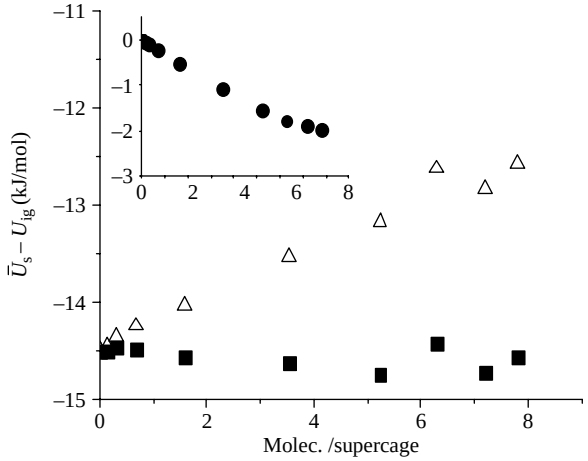

Figure 12. Same as Figure 11 for CH_4 in NaX at 300 K.

cosine law that ensures equal flux of the emitted molecules from the surface through any elementary area surrounding the collision point, irrespective of the direction. In this way, it is ensured that the probability for a molecule to leave the surface per unit time per unit area on the surface increases as the angle of reflection approaches the normal to the surface.

The left-hand side of Figure 9 shows the high-pressure regime ($\langle l \rangle = \lambda$), where the overall diffusion process is controlled by frequent intermolecular collisions, and the right-hand side of the same graph shows the behaviour in the low-pressure regime, where molecular collisions with the surfaces of NaX crystals in the bed dominate the overall diffusion process and mean free paths are long ($\langle l \rangle \ll \lambda$); obviously in the latter regime, for λ values higher than $\langle l \rangle$, which in this case represents the mean chord length of the zeolite bed, inter-crystalline diffusivity remains unaltered (see plateau in Figure 9).

The results of Figure 10 for deuterium show a different trend from that observed with methane. Here, both quasi-elastic incoherent neutron scattering and MD reveal an increase in the self-diffusivity of deuterium at low densities, followed by a plateau up to eight molecules per supercage of NaX.

This behaviour may be explained on the basis of the different guest–host interactions for deuterium and methane (cf. Figures 11 and 12). These differences are reflected in the partial molar configurational internal energy of the sorbed species (i.e. devoid of the kinetic energy part, U_{ig}), $\bar{U}_s - U_{ig}$, as obtained from the covariance between the number of molecules and potential

energy, divided by the variance in the number of molecules in the course of a GCMC simulation, i.e.

$$\bar{U}_s - U_{ig} = \frac{\langle NU \rangle - \langle N \rangle \langle U \rangle}{\langle N^2 \rangle - \langle N \rangle^2}. \tag{14}$$

In particular, it is seen that the total partial molar configurational internal energy increases abruptly in the case of deuterium and then decreases slightly as loading increases. Although in methane the net host–guest interactions exhibit a steady increase with loading, the total partial molar configurational internal energy of sorbed molecules remains almost constant; this is because the methane–methane part of the partial molar configurational energy decreases much faster with occupancy compared with the sorbed deuterium–deuterium interactions (cf. insets in Figures 11 and 12). As a consequence, hydrogen perceives a higher energetic heterogeneity within NaX than does methane. The most attractive host sites (i.e. those presenting the deepest minima in the host-hydrogen potential energy field) are occupied first, the molecules residing in them being less mobile; additional molecules at higher occupancy are more loosely bound. Thus, an increase in deuterium loading is accompanied by an increase in self-diffusivity (Figure 10). On the other hand, methane, which feels a practically homogeneous energetic environment, exhibits a decrease in self-diffusivity with loading because of enhanced intermolecular collisions at high loadings (Figure 8). The above observed difference in host–guest interactions for the two molecules gives rise to opposite trends in the concentration dependence of self-diffusivities.

In a simulation study on ITQ-1, we found a shallow maximum with occupancy in the self-diffusivity of methane. In this zeolite, the pore structure is more complicated than the one of NaX, with two disconnected pore systems. Two-dimensional diffusion can occur in each pore system with the D_{zz} element of the diffusivity tensor being zero. One pore system exhibits large cavities communicating through narrow necks (Figure 4). In this type of structure, we found that the concentration dependence of the self-diffusivity can be strongly affected by the sorbate density distribution along the narrow interconnections [25]. Figure 13 shows such a sequence

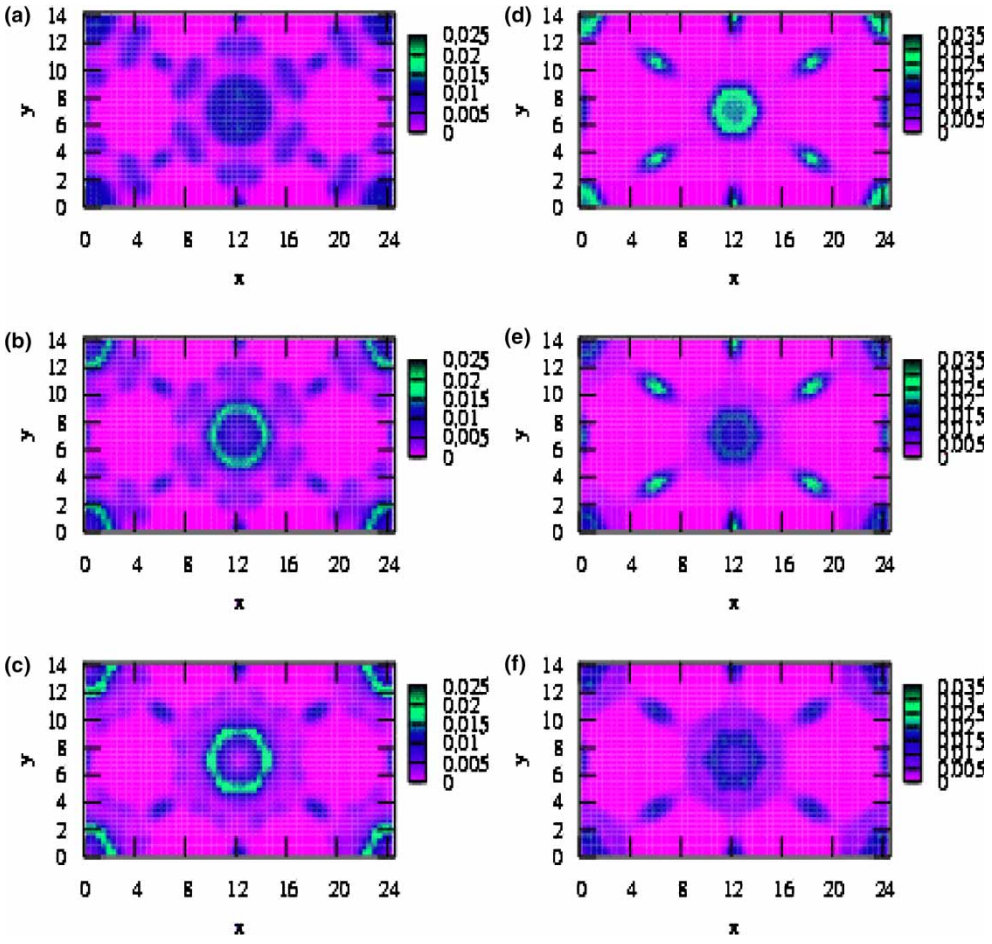

Figure 13. *xy* probability densities for CO_2 (a, b, c) and CH_4 (d, e, f) sorbates in the LC pore system of ITQ-1 at $T = 250$ K. The pressure is 0.006 atm (a, d), 0.95 atm (b, e) and 52 atm (c, f).

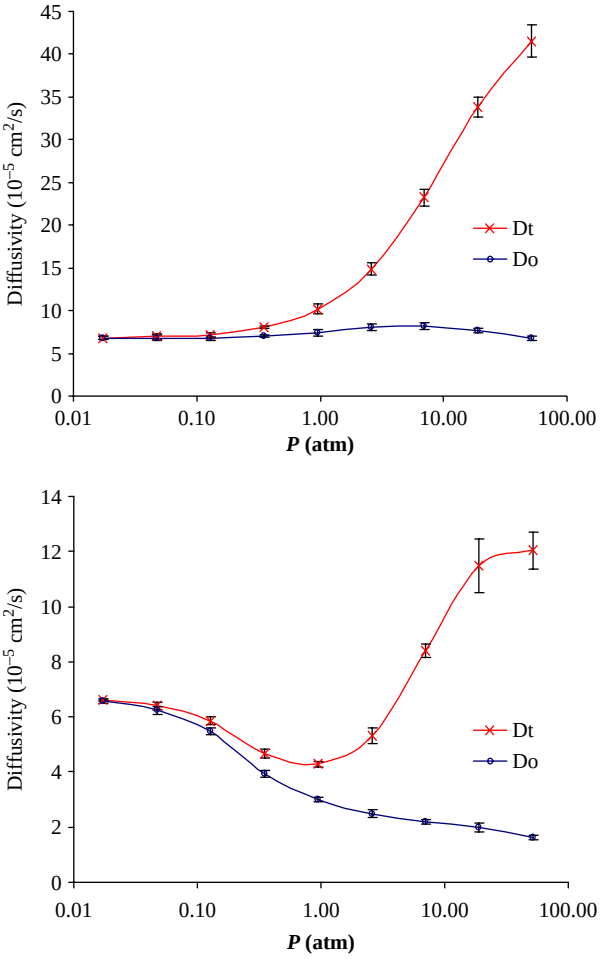

Figure 14. Collective and transport diffusivities at 300 K for CH_4 (top) and CO_2 (bottom) in ITQ-1 as a function of pressure of the bulk phase at equilibrium.

of computed probability densities for CO_2 and CH_4 for various total concentrations inside the ITQ-1 crystal. Methane prefers to reside at the top and bottom of the large cavities. As occupancy increases, it tends to occupy the middle regions of the large cavities more; this facilitates entry into and passage through the narrow necks emanating from the middle regions of the large cavities (Figure 4), leading to the observed shallow maximum in self-diffusivity [25].

In Figure 14, the collective (or else the Maxwell–Stefan [17]) diffusivity and the transport diffusivity of methane and carbon dioxide in ITQ-1 are presented. The observed behaviour for carbon dioxide is a continuous decrease in collective diffusivity as the fugacity (pressure of bulk phase) of the sorbed phase increases. On the other hand, methane exhibits a slight maximum.

The effect of concentration on the collective diffusivity of hydrogen in NaX is presented in Figure 15; in this graph, contrary to the trend observed for methane in the same zeolite, collective diffusivity shows initially

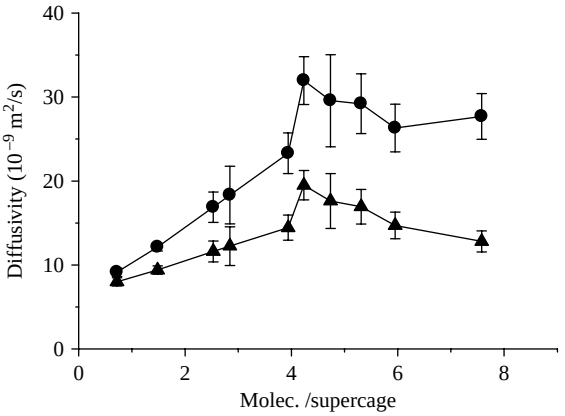

Figure 15. Collective (triangles) and transport (circles) diffusion coefficients predicted via MD as a function of H_2 loading in NaX.

an increase up to a slight maximum just beyond four molecules per supercage. In order to interpret this behaviour, we have previously invoked the Reed and Ehrlich theory [26], according to which the occupancy dependence of the collective (or corrected, or else Maxwell–Stefan) diffusivity can be related to the strength of interactions between the sorbate molecules. In the lattice model considered by Reed and Ehrlich, this strength is quantified through the nearest neighbour interaction energy parameter, w, introduced in conjunction with the quasi-chemical mean field theory of sorption; the coordination number, z, of the lattice and the saturation capacity, ρ_m, are additional parameters of the model [5,26].

Figure 16 gives an indicative example of the use of Reed–Ehrlich theory for the case of hydrogen in NaX. The parameters w and z were estimated by means of fitting to the simulation data; ρ_m was computed by GCMC. According to this simple theory, the presence of a maximum in the collective diffusivity is a consequence of a weak (considerably less than k_BT) dispersion interaction between co-sorbed hydrogen molecules. In the same graph is shown the predicted collective diffusivity of deuterium; this is described better by the theoretical Reed and Ehrlich curve. The differences seen between H_2 and D_2 in Figure 16 correspond to more attractive sorbate–sorbate interactions between D_2 molecules when compared with H_2 molecules.

Figure 17 shows three other theoretical plots based on the Reed and Ehrlich theory, constructed for more attractive sorbate–sorbate interactions. These exhibit completely different loading dependences that are reminiscent of the behaviours of methane and carbon dioxide in ITQ-1 (Figure 14). One should note that the model of jumps in a lattice considered by Reed and Ehrlich theory is very simplified, providing only a qualitative

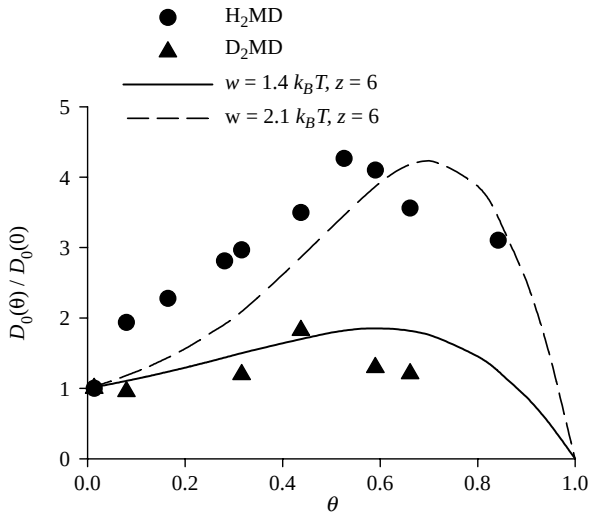

Figure 16. Normalised simulated and experimental collective diffusivities for hydrogen (circles) and deuterium (triangles) in NaX versus fractional occupancies $\theta = \rho/\rho_m$, where ρ_m is the saturation capacity of NaX for H_2; lines correspond to theoretical predictions from the Reed and Ehrlich model [26].

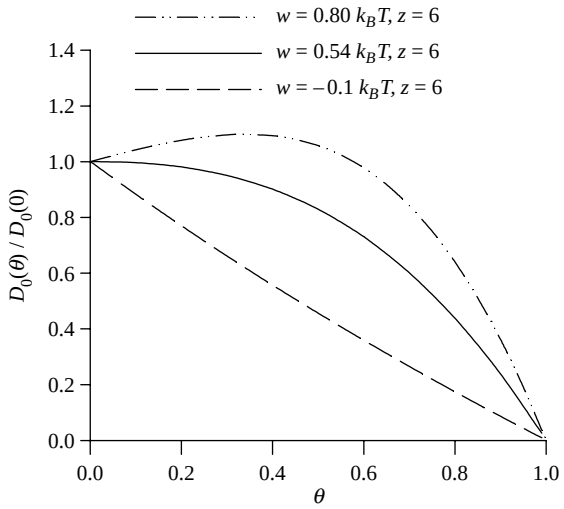

Figure 17. Normalised collective diffusivities versus fractional occupancies θ for various w values corresponding to theoretical predictions from the Reed and Ehrlich model [26].

explanation of the occupancy dependence of the collective diffusivity of fluids under confinement.

4. Conclusions

We have performed simulations at atomistic and mesoscopic levels in order to explore the concentration dependence of the sorbed phase dynamics of polar and non-polar fluids in digitally reconstructed purely siliceous as well as counterion-containing aluminosilicate zeolite frameworks.

For the former category, we selected a typical representative belonging to framework-type code MWW, the ITQ-1. Sorption and diffusion in this zeolite should differ only slightly from those in the protonated version of its aluminium-containing analogue, MCM-22. In the latter class, a representative of the FAU framework type, $Na_{86}X$, was reconstructed. The Si/Al ratio in the frame of this type determines the anionic charge, and therefore the number of cations (counterions) per unit cell. It also affects the distribution of counterions among the various kinds of sites present in the unit cell. In the modelling distinct Coulombic charges were attributed to all atoms in the framework.

Our MD results for the self-diffusivity of methane in NaX show that D_s decreases as the loading increases; this is in agreement with earlier PFG-NMR intra-crystalline self-diffusivity measurements of other groups [22,23]. Furthermore, our KMC mesoscopic simulations of inter-crystalline diffusion in an assemblage of NaX crystals predict that the inter-crystalline diffusivity, not captured by atomistic MD simulations, becomes important at high temperatures where Knudsen diffusion becomes dominant.

The self-diffusivity of deuterium in NaX, which is predicted in good agreement with recent QENS measurements, exhibits a monotonic increase with loading. The energetic heterogeneity experienced by deuterium molecules in NaX proves to be responsible for this peculiar behaviour, also observed in the case of hydrogen in NaX. Within ITQ-1, which possesses large elongated cavities with strongly attractive regions at their top and bottom, connected along their waists by narrow, strongly attractive pores, the self-diffusivity of methane exhibits a shallow maximum. A mesoscopic diffusion through spatial discretisation approach recently developed in our group [25] is able to explain this trend.

Collective (Maxwell–Stefan) and transport diffusivities of carbon dioxide and methane in ITQ-1 and also of hydrogen and deuterium in NaX were studied via atomistic MD simulations. Their concentration dependence was investigated on the basis of the sorbate–sorbate interaction strength invoked by quasi-chemical mean field theory in conjunction with the simple model of Reed and Ehrlich.

Acknowledgements

We are grateful to Dr E. Pantatosaki and Mr M. Sant for their contribution in the computational work. Support by the European Union via the FP6-Marie Curie Research Training Network 'INDENS' (MRTN-CT-2004-005503) is gratefully acknowledged.

Note

1. Email: gkpap@chemeng.ntua.gr

References

[1] D.N. Theodorou, R.Q. Snurr, and A.T. Bell, *Molecular dynamics and diffusion in microporous materials*, in *Comprehensive Supramolecular Chemistry*, G. Alberti and T. Bein, eds., Vol. 7, Elsevier, Oxford, 1996, pp. 507–548.

[2] S.M. Auerbach, F. Jousse, and D.P. Vercauteren, *Dynamics of sorbed molecules in zeolites*, *Computer Modelling of Microporous and Mesoporous Materials*, C. R. A. Catlow, R. A. van Santen and B. Smit, eds., Elsevier, Amsterdam, 2004, pp. 49–108.

[3] G.K. Papadopoulos and D.N. Theodorou, *Computer simulation of sorption and transport in zeolites*, in *Handbook of Heterogeneous Catalysis*, G. Ertl, H. Knözinger, F. Schüth and J. Weitkamp, eds.,Vol. 3, 2nd ed., Wiley-VCH, Weinheim, 2008, pp. 1662–1676.

[4] J.P. Hansen and I.R. McDonald, *Theory of Simple Liquids*, Academic Press, London, 1986.

[5] G.K. Papadopoulos, H. Jobic, and N. Theodorou, *Transport diffusivity of N_2 and CO_2 in silicalite: Coherent quasielastic neutron scattering measurements and molecular dynamics simulations*, J. Phys. Chem. B 108 (2004), pp. 12748–12756.

[6] G.K. Papadopoulos, *Diffusivity of CH_4 in model silica nanopores: Molecular dynamics and quasichemical mean field theory*, Mol. Simul. 31 (2005), pp. 57–66.

[7] A. Kumar, H. Jobic, and K. Bhatia, *Quantum effects on adsorption and diffusion of hydrogen and deuterium in microporous materials*, J. Phys. Chem. B 110 (2006), pp. 16666–16671.

[8] G.K. Papadopoulos, D.N. Theodorou, S. Vasenkov, and J. Kärger, *Mesoscopic simulations of the diffusivity of ethane in beds of NaX zeolite crystals: Comparison with pulsed field gradient NMR measurements*, J. Chem. Phys. 126 (2007), 094702.

[9] E. Pantatosaki, G.K. Papadopoulos, H. Jobic, and D.N. Theodorou, *A combined atomistic simulation and quasielastic neutron scattering study of the low-temperature dynamics of hydrogen and deuterium confined in NaX zeolite*, J. Phys. Chem. B 112 (2008), pp. 11708–11715.

[10] E. Pantatosaki and G.K. Papadopoulos, *On the computation of long-range interactions in fluids under confinement: application to pore systems with various types of spatial periodicity*, J. Chem. Phys. 127 (2007), 164723.

[11] J.-M. Leyssale, G.K. Papadopoulos, and D.N. Theodorou, *Sorption thermodynamics of CO_2, CH_4 and their mixtures in the ITQ-1 zeolite as revealed by molecular simulations*, J. Phys. Chem. B 110 (2006), pp. 22742–22753.

[12] D.E. Jaramillo and S.M. Auerbach, *New force field for Na cations in faujasite-type zeolites*, J. Phys. Chem. B 103 (1999), pp. 9589–9594.

[13] K. Makrodimitris, G.K. Papadopoulos, and D.N. Theodorou, *Prediction of permeation properties of CO_2 and N_2 through silicalite via molecular simulations*, J. Phys. Chem. B 105 (2001), pp. 777–788, and references therein.

[14] E.V. Chkhaidze, A.A. Fomkin, V.V. Sepinskii, and G.V. Tsitsishvili, *Adsorption of methane on NaX zeolite in the subcritical and supercritical regions*, Bull. Acad. Sci. USSR, Div. Chem. Sci. 34 (1985), pp. 886–890.

[15] R.P. Feynman and A.R. Hibbs, *Quantum Mechanics and Path Integrals*, McGraw-Hill, New York, 1965.

[16] D. Fincham, *Leapfrog rotational algorithms for linear molecules*, Mol. Simul. 11 (1993), pp. 79–89.

[17] D. Dubbeldam and R.Q. Snurr, *Recent developments in the molecular modeling of diffusion in nanoporous materials*, Mol. Simul. 33 (2007), pp. 305–325.

[18] R. Krishna and J.M. van Baten, *Onsager coefficients for binary mixture diffusion in nanopores*, Chem. Eng. Sci 63 (2008), pp. 3120–3140.

[19] S.J. Goodbody, K. Watanabe, D. MacGovan, J. Walton, and N. Quirke, *Molecular simulation of methane and butane in silicalite*, J. Chem. Soc. Faraday Trans. 87 (1991), pp. 1951–1958.

[20] D. Dubbeldam, S. Calero, T.J.H. Vlugt, R. Krishna, T. Maesen, and B. Smit, *United atom force field for alkanes in nanoporous materials*, J. Phys. Chem. B 108 (2004), pp. 12301–12313.

[21] J.G. Harris and K.H. Yung, *Carbon dioxide's liquid–vapor coexistence curve and critical properties as predicted by a simple molecular model*, J. Phys. Chem. 99 (1995), pp. 12021–12024.

[22] J. Kärger, H. Pfeifer, M. Rauscher, and A. Walter, *Self-diffusion of n-paraffins in NaX zeolite*, J. Chem. Soc. Faraday Trans. 76 (1980), pp. 717–737.

[23] J. Caro, M. Bülow, and W. Schirmer, *Microdynamics of methane, ethane and propane in ZSM-5 type zeolites*, J. Chem. Soc. Faraday Trans. 81 (1985), pp. 2541–2550.

[24] O. Geier, S. Vasenkov, E. Lehmann, J. Kärger, U. Schemmert, R. Rakoczy, and J. Weitkamp, *Interference microscopy investigation of the influence of regular intergrowth effects in MFI-type zeolites on molecular uptake*, J. Phys. Chem. B 105 (2001), pp. 10217–10222.

[25] M. Sant, G.K. Papadopoulos, and D.N. Theodorou, *A second-order Markov process for modeling diffusive motion through spatial discretization*, J. Chem. Phys. 128 (2008), 024504; M. Sant, J.-M. Leyssale, G.K. Papadopoulos, and D.N. Theodorou; in preparation.

[26] D.A. Reed and G. Ehrlich, *Surface diffusion, atomic jump rates and thermodynamics*, Surface Sci. 102 (1981), pp. 588–609.